

Detection of brine plumes in an oil reservoir using the geoelectric method

This article has been downloaded from IOPscience. Please scroll down to see the full text article.

2013 J. Geophys. Eng. 10 045006

(<http://iopscience.iop.org/1742-2140/10/4/045006>)

View [the table of contents for this issue](#), or go to the [journal homepage](#) for more

Download details:

IP Address: 157.92.4.71

The article was downloaded on 03/07/2013 at 22:10

Please note that [terms and conditions apply](#).

Detection of brine plumes in an oil reservoir using the geoelectric method

María Victoria Bongiovanni¹, Ana Osella², Matías de la Vega²
and Adrián Tichno³

¹ Facultad de Ingeniería-Universidad Austral/CONICET, Buenos Aires, Argentina

² Departamento de Física, Facultad de Ciencias Exactas y Naturales, Universidad de Buenos Aires, IFIBA/CONICET, Buenos Aires, Argentina

³ INLAB S.A., Buenos Aires, Argentina

E-mail: mbongiovanni@austral.edu.ar

Received 20 December 2012

Accepted for publication 28 May 2013

Published 2 July 2013

Online at stacks.iop.org/JGE/10/045006

Abstract

During water injection in a reservoir at the secondary recovery phase, oil is replaced by salt water, producing different saturation zones in the formation containing this reservoir. This process could be optimized if the direction of the fluids is monitored. Since there are large contrasts in the electric conductivity between salt water and oil, geoelectrical methods could provide a water saturation map at any given moment of the production. The case we study here corresponds to a rather shallow reservoir (between 500 and 600 m in depth). As the wells are in production, electrodes for borehole measurements cannot be introduced. Hence, our objectives are to determine the possibilities of detecting the channelling direction of saline water between injection and producing wells, and applying the method of placing electrodes on the surface or even burying them, but at depths corresponding to shallow layers. We design an electrical model of the reservoir and then numerically simulate the geoelectrical response in order to determine the conditions under which the anomaly, i.e. the accumulation of brine in a reduced area, can be detected. We find that the channelling of the brine can be detected for the reservoir studied here if the electrodes are placed at 180 m depth. The Wenner configuration using 16 electrodes provides the best resolution. Therefore, monitoring the voltage at a number of electrodes embedded at rather shallow depths (from a technical-logistic point of view) could give information about the direction of the saline channelling even if a quantitative image of the subsoil cannot be obtained due to the reduced number of electrodes used in the study.

Keywords: brine plumes, geoelectric, oil recovery, numerical modelling

(Some figures may appear in colour only in the online journal)

Introduction

An oil field is a porous volume containing oil, water and often a gaseous phase, supported by a geological structure that does not allow these products to escape to the surface. The oil is confined in a porous medium of sedimentary origin such as sandstone or limestone with different degrees of consolidation.

Changes occurring during the long process of sedimentation make the porous medium often heterogeneous, both microscopically and macroscopically, and small

permeable areas and eventually fracture levels are produced. Inhomogeneities complicate production operations because they tend to produce preferential paths for the flow of fluids.

Traditionally, three steps can be distinguished during the exploitation of a deposit: primary recovery, secondary recovery and tertiary, assisted or enhanced oil recovery (EOR). This last technique usually implies the injection of carbon dioxide (CO₂), solvents, polymers, or thermal methods such as the injection of steam, or combustion *in situ*. Due to its high

cost, this phase is carried out when the prices of crude oil are economically feasible (e.g., Donaldson *et al* 1989).

During primary recovery, oil drains naturally to the wells under the effect of the gradient of pressure. The primary recovery period has a variable duration, allowing collection of a great deal of information about the behaviour of the site, which is important for planning further exploitation. The primary recovery ends when the pressure of the reservoir has fallen too much, or when they are producing too large quantities of other fluids (gas, water). This usually occurs when only 8 or 10% of the oil has been extracted.

Secondary recovery methods involve the injection of fluids (that are cheaper than oil, e.g. water, or water with additives, gas and/or a combination of these) to maintain the pressure gradient. These fluids are injected by certain wells (injectors), and move or drag a portion of the oil into the other wells (producers). The gradual recovery of oil is obtained only with the movement of large volumes of water. As the water that pushes the oil has lower viscosity than the oil, its mobility in the porous medium is higher, and given the typical heterogeneity of rocks, it forms channels through which water flows faster than the oil. This process produces a reduction in oil production with respect to the water production, which must be re-injected. When the injection of water ceases to be effective due to only a small extraction of crude oil, the tertiary or recovery treatment of the oil well begins. After secondary recovery is completed, 65–75% of the initial hydrocarbon still remains at the site (Lake 1992).

Within the secondary exploitation, and before entering the much more expensive tertiary recovery process, there are various techniques that are used to look for improving the recovery of oil.

The goal of some of these techniques is to seal high permeability channels through the injection of gels or changing the water and oil viscosity with polymers and surfactants. Also, to change the injection–extraction pattern changing the injection to extraction wells function or varying the injection caudal and in some cases increasing the intermediate well density. In any case, it would be of interest to know, with some degree of accuracy, the salt water content at all points of the production layer of the reservoir at any given moment of its production history. With these data it is possible to optimize the use of any of these techniques and to control their application.

There are different methods to verify the connectivity between the different wells: tracer measurements, radioactive or organic; pressure testing; etc.

During the water injection in the secondary recovery phase, the oil is replaced by salt water. There are large contrasts in density and electric conductivity between the salt water and the oil. Hence, salt water zones can be mapped at any given moment of the production by applying geoelectrical methods. We study the feasibility of using this geophysical method as a tool for detecting areas of different salt water content within the same productive layer of a reservoir.

This study was conducted with the aim of applying the results to a rather shallow reservoir (between 500 and 600 m in depth). A usual practice is to place the electrodes inside the well for borehole measurements (for example as described in

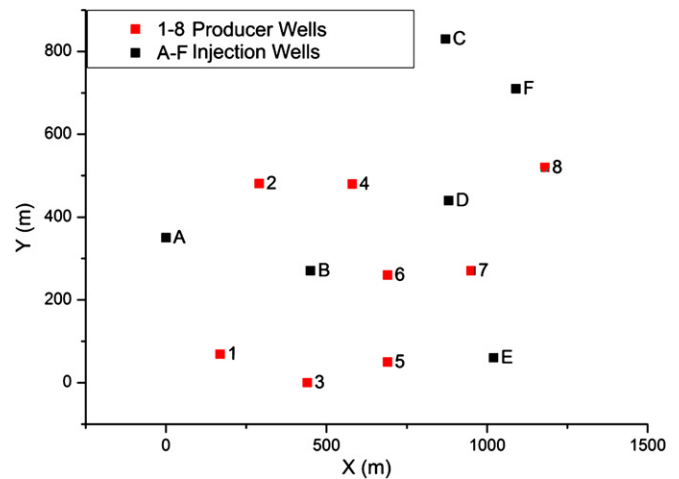


Figure 1. Schematic map with the location of injection and production wells.

Picotti *et al* (2013)) or for surface-borehole measurements (e.g. Bergmann *et al* 2012). In the present case, as the production in wells cannot be stopped, it is not possible to place electrodes inside the wells. Therefore, the objective of our work is to determine the possibilities of detecting the channels of saline water between injection and producing wells, by placing electrodes on the surface or even burying them, but at depths corresponding to shallow layers.

As a first step we built an electrical model comprising borehole data and geological information. We numerically simulated the geoelectrical responses for different configurations using the Abaqus (2009)⁴ code, which is a general-purpose finite element program which can be used to calculate physical responses of a medium characterized by a refined mesh, supporting a large number of cells. This is a necessary requirement for this particular case, since we are looking for an electrical anomaly whose dimensions are much smaller than its depth. Furthermore, if the sedimentary basin has a high content of clay and salt water, then the sedimentary matrix is much conductive, with resistivity values that in general do not reach more than 20–30 Ωm . This feature makes the problem even more difficult to solve. We performed sensitivity analysis, varying the electrode deployment, in order to look for a configuration with fewer electrodes and located at the shallowest depth which allows mapping the water saturated zones, and that, at the same time, is economically feasible.

Electrical modelling of the reservoir

We worked on an oil reservoir whose depth is about 500 m, located in the western region of Argentina. This reservoir is under recovery operations and we focused our study on an area of approximately 1 km², where there are six injection wells and eight production wells (figure 1). The mean distance between wells is 300 m.

⁴ Abaqus 6.9 Unified Finite Element System, 2009. Dassault Systèmes Simulia Corp., Rising Sun Mills, 166 Valley Street, Providence, RI, USA. <www.simulia.com>

In order to numerically simulate the geoelectrical responses, the first step was to build an electrical model of the reservoir. We used data from boreholes acquired when drilling and their geological interpretation. The top of the formation corresponding to the reservoir (we named it F) extends from approximately 475 to 515 m depth, depending on the location of the wells. Different data obtained from the wells during the drilling (types of sandstones, porosity, permeability, initial water and oil saturations, and electrical logs) enabled four sub-layers within the formation to be recognized. The two upper sub-layers and the bottom of the formation presented discontinuities due to their depositional characteristics and only the third sub-layer had a continuous horizon, constituting the exploited reservoir.

In figure 2 we show as an example the electrical log corresponding to one of the wells together with the sandstone and clay distribution, confirmed through different punctures.

This initial composition changes as saline water flows through the porous sandstones, producing channelling patterns which depend on the permeability contrasts of the layer as well as on the dynamics of the injection procedures in the field. Puncturing in different wells showed that the permeable layer may extend between 483 m and 534 m depth, corresponding to a 6.15 m mean-thickness of sandstone and the remainder formed by sandstone with intercalated clays.

In order to assign an adequate resistivity value we used Archie's law (Archie 1942), which gives the relation between the real resistivity of a rock and its water content:

$$R_t = a\phi^{-m}S_w^{-n}R_w, \quad (1)$$

where R_t and R_w are the resistivity of the rock partially filled with water and of the water alone, respectively; ϕ is the porosity of the rock; S_w is the fraction of the pore volume filled with water; m is the cementation factor; n is the saturation exponent; and a is the tortuosity factor.

We used the values $a = 0.62$, and $m = 2.15$ as given by the Humble formula for the formation factor applicable to many granular rocks (Telford 1990). Also, a value of $n = 2$ was used (Telford 1990).

Data obtained from the wells showed that the porosity of the formation lies between 25 and 30%. The brine concentration was 30 000 ppm. The brine resistivity at a depth of 500 m with a temperature of around 40 °C is 0.15 Ωm (Serra 1984).

After the primary and secondary oil extraction there is about 75 to 65% of oil remaining in the formation. We suppose that the pore space left free is occupied completely by the brine. That is to say there is between 25 and 35% respectively of the pore volume filled with brine. Therefore S_w takes a value between 0.25 and 0.35. With these values, using Archie's law, the formation resistivity takes a value between 14 and 29 Ωm.

Joining this information with the electrical values obtained from the electrical logs, we built up the layered model shown in figure 3. A first resistive layer (A) with a mean value of $\rho = 300 \Omega\text{m}$, two layers of $\rho = 20 \Omega\text{m}$ and $\rho = 7 \Omega\text{m}$, (B and C, respectively) and below it a layer of $\rho = 4 \Omega\text{m}$ (D), corresponding to the caprock, the impermeable layer mainly composed of clays, whose top is about 300 m and bottom at

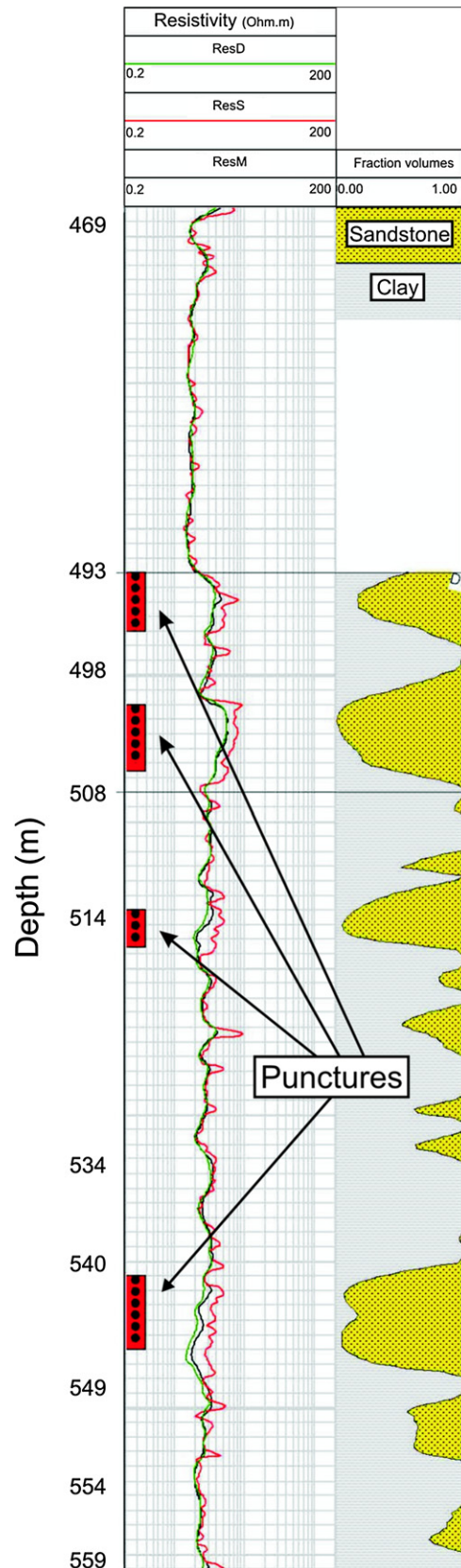


Figure 2. Electrical profile with shallow, medium and deep resistivity (ResS, ResM, ResD) in Ω.m on a logarithmic scale, corresponding to one of the wells. The position of punctures and fractions of clay and sandstone in the total volume are also shown.

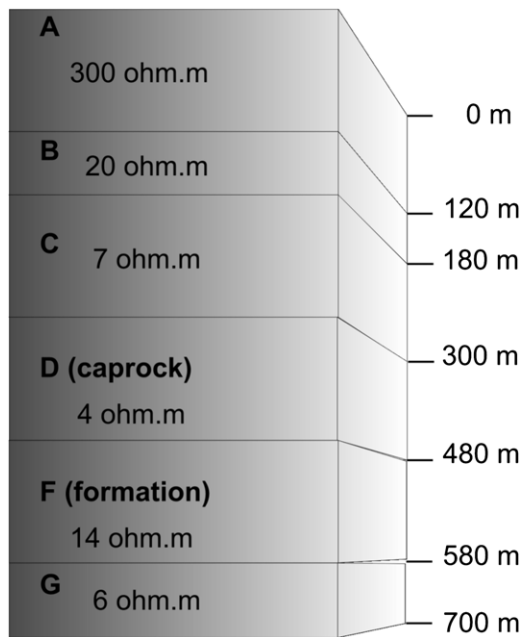


Figure 3. Electrical modelling of the reservoir, F corresponds to the formation containing the reservoir. Depths and electrical resistivities of each layer were obtained from electrical logs and geological information.

approximately 480 m. At this depth the layer corresponding to the reservoir Formation (F) begins with a mean value of $\rho = 14 \Omega\text{m}$, and a thickness of 100 m. We located the bottom of the continuous horizon which defines the reservoir at 530 m, and then the anomaly associated with the injected saline water is placed at this depth. Finally, the model is completed with a last layer G of $\rho = 6 \Omega\text{m}$.

This model is representative of the electrical distribution of the area, in the absence of brine channels.

To model the channelling of the brine, we assume a very conductive body, centred in the continuous horizon of layer F. We suppose that the pore space is completely occupied with brine ($S_w = 1$) and there is an effective porosity of 0.9. With these values, using Archie's law, the formation resistivity channel zones take a value of $0.12 \Omega\text{m}$. Nevertheless, as our aim is to find limits of detectability, in our numerical models the resistivity values were varied between 0.05 and $5 \Omega\text{m}$ for the channel zone. This was done to study the possibility of detecting the channels using different brine concentrations. Its dimensions (area and thickness) were also varied in order to study the sensitivity in the detection of the anomaly.

Geoelectrical 3D forward modelling

At this stage, we have to numerically simulate the geoelectrical response of the model in order to determine the conditions under which the anomaly, i.e. the accumulation of brine in a reduced area, can be detected. We have to keep in mind that the primary objective of this work is to study the possibilities of detecting the direction of the water flow after being injected through punctures in the injection well. Then the problem we have to solve is a case of a very conductive anomaly, embedded in an also conductive medium, and whose dimensions (area and

thickness) should be much less than the depth at which it is located.

The usual modelling codes use finite elements or finite differences to calculate the electrical potential at the points where the electrodes are placed, with the constraint that the density of the grid cannot be freely varied. We have to take into account that the anomaly may have a thickness of no more than 5–6 m and a lateral extension of some tens of metres; these characteristics mean that the grid needs to be dense enough to resolve the geometry. The problem arises because it is located at about 500 m depth. The usual methods allow varying the size of the cells only restrictively, therefore the number of elements should be large to resolve the target, overpassing the limits of these methods. These are the main reasons why we decided to test the Abaqus code as an alternative to solve this problem. This is a general-purpose finite element program which can be used to calculate physical responses of media characterized by a refined mesh, supporting a large number of cells.

The application was adapted to calculate the electrical potential in the medium produced by the injection of dc current by means of a pair of point sources (usually named electrodes A and B). Potential electrodes are named M and N, and then V_{MN} is the potential difference between these two electrodes. The mesh was designed according to the electrical model described in figure 3, covering an area of $3 \times 3 \text{ km}^2$. The anomaly was modelled as a parallelepiped whose bottom was placed at 530 m; the lateral dimensions were varied from $100 \times 100 \text{ m}^2$ to $3 \times 3 \text{ km}^2$ (i.e. a conductive thin sheet) and the thickness from 8 m to 60 m in order to analyse its detectability. We used rectangular cells due to the geometry proposed for modelling the anomaly, and with a larger density of cells in the region close to its location. The number of cells depended on the geometrical dimensions of the anomaly and on the position of the electrodes, but typically the mesh was designed with approximately 260 000 elements.

For simulating the geoelectric response that should be obtained in the field, we used four different electrode configurations; Wenner, Schlumberger, pole–pole and pole–dipole (see e.g. Reynolds 1997). For each position of electrodes A and B (according to the selected configuration), the distribution of the electrical potential over the plane where these electrodes were placed was calculated for both models: the layered media with and without the anomaly. With the results, the differences in the potential at the nodes corresponding to the position of the potential electrodes between both models ($\Delta V_{MN} = V_{MN_A} - V_{MN_L}$, where V_{MN_A} and V_{MN_L} are the potentials with and without the anomaly, respectively) were determined. For each configuration, we look for the minimum depth at which the buried electrodes detected the anomaly. We considered V_{MN_A} and V_{MN_L} with an error of 5%. With this error we numerically observed that $(V_{MN_A} - V_{MN_L}) > 10 \text{ mV}$ was a good criterion to differentiate the two data values.

Electrode configurations

As a first approach, different tests were made to analyse the conditions required in order to detect the anomaly when

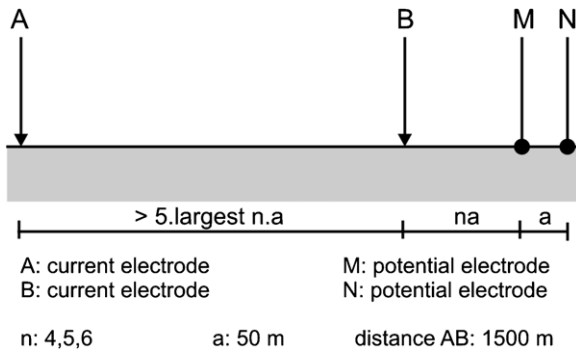


Figure 4. Survey procedure using a pole–dipole array. The electrodes A, M and N remain fixed while B is shifted for each value of n . We used six electrodes; five at 400 m depth and one on the surface (A).

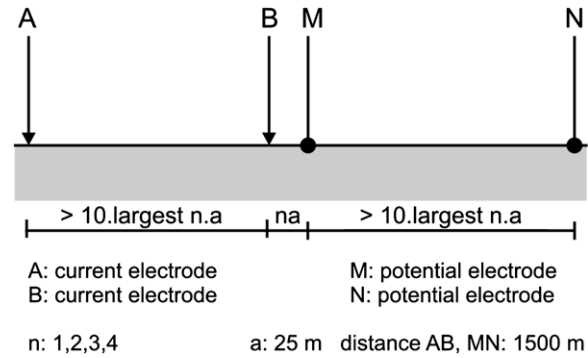


Figure 5. Survey procedure using a pole–pole array. The electrodes A, M and N remain fixed while B is shifted for each value of n . We used seven electrodes; five at 400 m depth and two on the surface (A and N).

Table 1. Cases in which the anomaly could be detected measuring on the surface, for different electrode configurations, for an anomaly with a lateral extension of 1 km and different thickness. RC is the relative conductivity of the anomaly with respect to the host medium.

Lateral extension	Thicknesses (m)	RC	Configuration
1 km	10	100	Pole–dipole
1 km	5	1000	Pole–dipole
1 km	60	10	Pole–dipole
1 km	10	100	Pole–pole
1 km	5	1000	Pole–pole
1 km	75	10	Pole–pole

measured at the surface. We varied the lateral extension of the anomaly, its thickness and its electrical resistivity, expressed in terms of relative conductivity of the brine with respect to the host medium ($RC = 10, 100$ and 1000 , respectively). The base of the anomaly is at a depth of 530 m. We summarize in table 1 some cases for which the anomaly was detectable. The minimum lateral extension was about 1 km, larger than the expected values of the brine channelling.

Then, we used electrodes buried in the subsurface to detect an anomaly with more realistic dimensions. For this, we choose configurations with a limited number of electrodes. The anomaly covered an area of $300 \times 325 \text{ m}^2$, and thickness of 8 m. The base of the anomaly in the simulation is as above at a depth of 530 m. We considered values of 10, 100 and 1000 for the RC. The responses were calculated using Wenner, Schlumberger, pole–dipole and pole–pole configurations (Edwards 1977).

Pole–pole and pole–dipole configurations

The mesh was designed taking into account the geometry of the electrical model and the position of the electrodes. We first calculated the distribution of the electrical potential at the depth where the electrodes are located. In order to analyse the effect of the anomaly we compared the response to the one produced by the layered model. From the numerical simulations of the potential distribution, we extracted the values of $V_{MN,A}$ and $V_{MN,L}$ at the positions corresponding to pole–pole and pole–dipole configuration. The survey procedures are shown in figures 4 and 5.

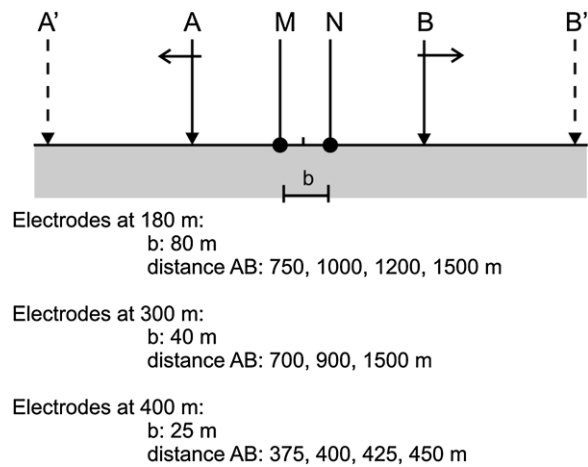


Figure 6. Survey procedure using Schlumberger array. The electrodes M and N remain fixed while A and B are shifted for each value of n . We used from eight to ten electrodes; all in depth.

One point to bear in mind is that the responses are not influenced by weather/environmental effects. As the electrodes are buried at a few hundreds of metres, the observed changes in the voltage should be due quite exclusively to the movements of fluids. Then, monitoring the voltage at a number of embedded electrodes could give information about the direction of the saline channelling even if we cannot quantitatively image the subsoil, provided that the difference in voltage can be large enough, at least 10 mV, to properly identify the event. The simulations were performed with the electrodes buried at a maximum depth of 400 m. We used the maximum value for the conductivity contrast, but did not find any detectable variation with the presence or absence of the conductive target.

Schlumberger configuration

The survey procedure is shown in figure 6. For this configuration, the apertures depend on the depth; AB separations decrease when the electrodes are placed deeper. We used ten electrodes and, as before, we calculated the different ΔV_{MN} between the models with and without the anomaly, for several values of AB, at different depths and assuming different

Table 2. Differences ΔV_{MN} between the models with and without anomaly, for Schlumberger configuration, varying injection and voltage electrode separation (AB and MN, respectively), at different depths. The relative conductivity, RC, was also varied. The anomaly covered an area of $300 \times 325 \text{ m}^2$, and thickness of 8 m. We used ten electrodes, except at 300 m, where we used eight.

Electrode depth (m)	RC	MN (m)	AB (m)	ΔV_{MN} (V)						
180	1000	80	750	0.070	1000	0.064	1200	0.064	1500	0.068
180	100	80	750	0.048	1000	0.046	1200	0.046	1500	0.048
180	10	80	750	0.010	1000	0.010	1200	0.012	1500	0.012
300	10	40	700	0.016	900	0.014	1500	0.008		
400	1000	25	375	0.840	400	0.676	425	0.648	450	0.686

Table 3. Differences ΔV_{MN} between the models with and without anomaly, for Wenner configuration, varying electrode separation at different depths. The relative conductivity, RC, was also varied. The anomaly covered an area of $300 \times 325 \text{ m}^2$, with a thickness of 8 m. We used 18 electrodes.

Electrode depth (m)	Relative conductivity	ΔV_{MN} (V)	ΔV_{MN} (V)	ΔV_{MN} (V)	ΔV_{MN} (V)	ΔV_{MN} (V)
		AB = 300 m MN = 100 m	AB = 600 m MN = 200 m	AB = 900 m MN = 300 m	AB = 1200 m MN = 400 m	AB = 1500 m MN = 500 m
0	1000	0	0	0	0	0.002
180	1000	0.038	0.102	0.166	0.194	0.180
180	100	0.028	0.072	0.118	0.138	0.128
180	10	0.006	0.018	0.030	0.034	0.032
300	10	0.028	0.060	0.072	0.074	0.062
400	1000	1.492	2.132	1.622	1.338	0.952

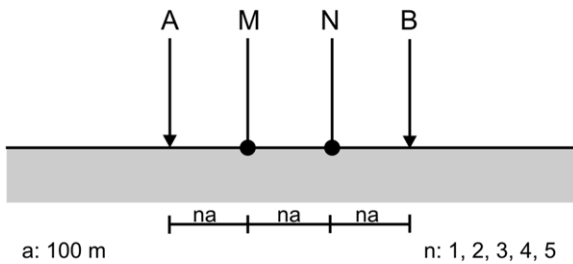


Figure 8. Survey procedure using Wenner array. The electrodes A, B, M and N are shifted for each value of n . We used 18 electrodes; all in depth.

in the large apertures required for the injection electrodes. And for $RC = 10$, even when the electrodes were at 300 m depth, the effect of the anomaly is hardly detected.

Wenner configuration

We simulated 18 electrodes, crossing the anomaly, with apertures na (distance between adjacent electrodes) of 100, 200, 300, 400 and 500 m, and placed at three different depths: 180, 300 and 400 m, respectively (see figure 8). The distance between adjacent electrodes gives current electrode separations (distance AB) of 300, 600, 900, 1200 and 1500 m. For each position of electrodes A and B, the distribution of the electrical potential over the plane where these electrodes were buried was calculated.

For this case the grid had 257 040 elements and computing times were about 3 h greater than for the Schlumberger case. In figure 7(b) we show, as an example, the mesh used for calculating the distribution of the electrical potential corresponding to the case of electrode positions at 300 m

depth, with the different apertures considered and RC equal to 1000. Then, for each position of electrodes A and B, the distributions of the electrical potential over the plane where these electrodes were buried (180, 300 and 400 m, respectively) were calculated.

We extract from the numerical simulations of the potential distribution, the values of $V_{MN,A}$ and $V_{MN,L}$ at the positions corresponding to the Wenner deployment. In table 3 a summary of the results obtained at different depths and with different values of RC are shown. We calculated the differences ΔV_{MN} between the models with and without anomaly, for the five distances AB considered. We also show the results when placing the electrodes on surface. For this case, even with maximum contrast ($RC = 1000$) the effect is not detectable. At a depth of 180 m, the anomaly can be detected if the conductivity of the anomaly is two or three orders larger than the host. If RC is 10, variations in the potential depend on the aperture of the electrodes, and for the lower separation the difference is negligible, but for larger apertures the anomaly can be detected. For this electrical contrast, embedding the electrodes at 300 m guaranteed variations of about 10 mV.

Discussion

In order to better illustrate the difference between the Wenner and Schlumberger configurations, we plot the differences ΔV_{MN} versus n for every survey and the limit of detectability of 10 mV (figure 9). These results show that a deployment using the Wenner configuration provides better results for detecting the anomaly. Clearly, the resolution will depend on the number of electrodes that can be buried, but it is important that by placing them at about 200 m, a measurable difference can be detected even for low contrast in the conductivities.

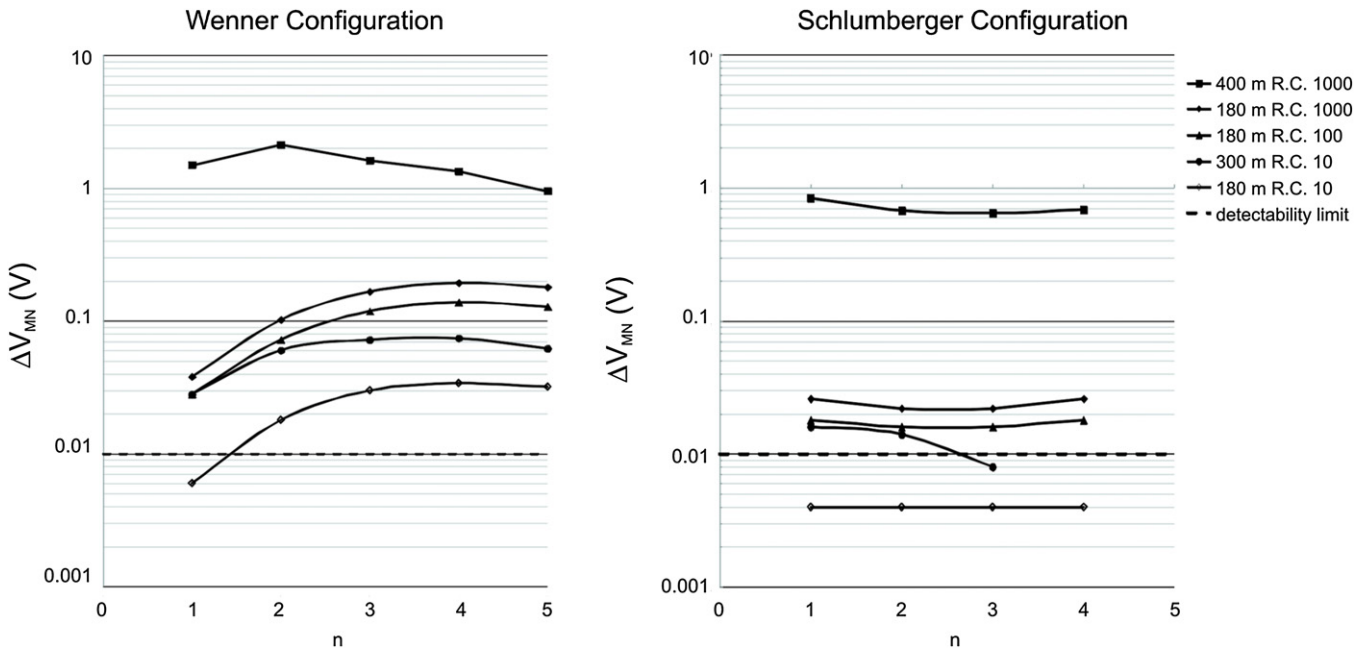


Figure 9. ΔV_{MN} versus n for Schlumberger and Wenner configurations showing the detectable cases.

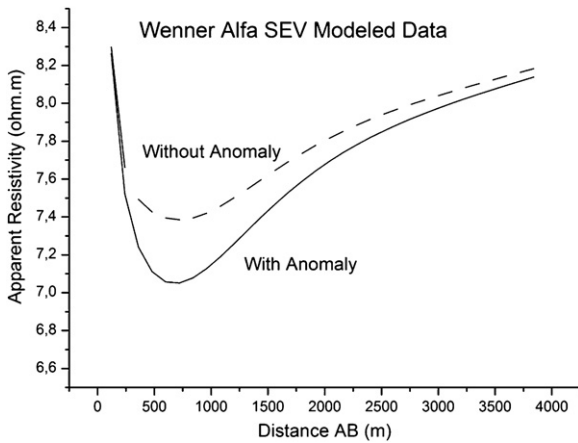


Figure 10. Synthetic Wenner vertical sounding for the layered model with and without the anomaly. RC = 1000 and the electrodes placed at 180 m depth.

We can simulate a Wenner vertical sounding (VES), supposing a larger number of electrodes, by extracting the data from the plan-views previously calculated, like the one shown in figure 7(b). We have to bear in mind that each view corresponds to the distribution of the potential for a fixed AB, so we have an output of the code for each AB, and with them we built up the VES. We make the calculations for the best scenario, RC = 1000, and the electrodes placed at 180 m depth. The resulting apparent resistivity curves, for the layered model with and without the anomaly, are shown in figure 10. Differences of 7% can be observed. These curves cannot be used for a quantitative analysis; the anomaly can be associated with a thin layer located at a depth much larger than its thickness, and in cases like this, the anomaly cannot be recovered when inverting VES

data. Anyway, we could qualitatively detect the modification in the conductivity that a variation in the fluid flow could introduce.

Conclusions

This analysis is an approach to the particular case that wells are in operation and permanent sensors have not been placed inside them. The options to apply the geoelectrical method to detect the channelling of brine would therefore be: (a) deploying the electrodes on surface, (b) placing them deeper but without reaching the depth of wells, or (c) making at least three wells and ERT simulations using borehole data. This last situation was not viable because there were operational and economic reasons which restricted drilling to depths close to that of the reservoir. Therefore the objective was to find feasible conditions for burying electrodes but at shallow depth. Then our goal was to find a configuration which uses the minimum number of buried electrodes located at the shallowest possible depths, with the additional constraint that, while electrical contrasts are high, however the environment was very conductive and therefore the injection of current was complicated, not guaranteeing large penetration.

Numerical simulations under these conditions could not be made using the usual forward modelling codes, because they are basically constrained by the design of the grids. So we decided to test the Abaqus software as an alternative code for the numerical simulations. We adapted this finite element program for calculating the electrical potential in a medium produced by the injection of dc current by means of a pair of point sources. In this way we could reproduce the geoelectrical response of the medium with a number of advantages with respect to other methods. We could design dense grids with

cells of variable dimension, depending on the location of the anomaly. As the code supports a large number of cells, we used up to 500 000 elements and achieved high definition in the earth model. Other important advantages are the possibilities of placing the injection electrodes at any place on the grid, not only on surface, and of modifying the amplitude of the injected current. In this sense the method proved to be very versatile, gave good resolution and calculating times were reasonable using a desktop PC.

As a methodology, we compared two profiles, one deployed for the layered earth (corresponding to the case where there are no saturated water flows) and the other located where possible channelling appears. We found that the channelling of the brine can be detected when the dimensions are similar to the separation between adjacent wells and if the electrodes are placed at least at 180 m depth. The Wenner configuration provided the best resolution. The applicability of this procedure will depend on the feasibility of embedding the electrodes. Anyway, taking into account that the direction of injection is known by the location of the punctures, preferred locations can be chosen for the profiles thus improving the resolution in the determination of the brine-flow. The deployment of the electrodes can be made covering different directions, allowing the detection of flow by comparing the data. Locating the electrodes at depth has the additional advantage of not being influenced by any external environmental effects (like rain, temperature). Hence monitoring changes in the responses can be directly associated with variations in fluid motions.

Acknowledgments

This work was partially supported by CONICET and ANPCyT. We thank Dr Jorge Argüello (from Petrobras Co.) for kindly providing us with the reservoir data that we have used in this work.

References

- Archie G E 1942 The electrical resistivity log as an aid in determining some reservoir characteristics *Pet. Trans. AIME* **146** 54–62
- Bermann P, Schmidt-Hatterberger C, Kiessling D, Rücker C, Labitzke T, Henniges J, Baumann G and Schütt H 2012 Surface-downhole electrical resistivity tomography applied to monitoring of CO₂ storage at Ketzin, Germany *Geophysics* **77** B253–67
- Donaldson E C, Chilingarian G V and Yen T F (ed) 1989 *Enhanced Oil Recovery, II—Processes and Operations, Developments in Petroleum Science* (Amsterdam: Elsevier Science Publishers) pp 129–419
- Edwards L S 1977 A modified pseudosection for resistivity and induced polarization *Geophysics* **42** 1020–36
- Lake L W (Editor in Chief) 1992 *Petroleum Engineering Handbook* (Pasadena, CA: Society of Petroleum Engineers) pp 621–7
- Picotti S, Gei D, Carcione J M, Grünhut V and Osella A 2013 Sensitivity analysis from single-well ERT simulations to image CO₂ migrations along wellbores *Leading Edge* **32** 504–12
- Reynolds J 1997 *An Introduction to Applied and Environmental Geophysics* (Chichester: Wiley) pp 1–778
- Serra O 1984 *Fundamentals of Well-log Interpretation: 1. The Acquisition of Logging Data* (Amsterdam: Elsevier) p 10
- Telford W M, Geldart L P and Sheriff R E 1990 *Applied Geophysics* 2nd edn (New York: Cambridge University Press) p 648